https://dx.doi.org/10.1016/j.jcsr.2020.106275

Determination of a full range constitutive model for high strength S690 steels

[1,2]Ho H.C., [1,2]Xiao M., [1,2]Hu Y.F., [1]Guo Y.B., [1,2]Chung K.F.*, [1,3]Yam M.C.H. and [1,2,4] Nethercot D.A.

[1]Department of Civil and Environmental Engineering,
The Hong Kong Polytechnic University, Hong Kong SAR, China.

[2]Chinese National Engineering Research Centre for Steel Construction (Hong Kong Branch),
The Hong Kong Polytechnic University, Hong Kong SAR, China.

[3]Department of Building and Real Estate,
The Hong Kong Polytechnic University, Hong Kong SAR, China.

[4]Department of Civil and Environmental Engineering, Imperial College London, U.K.

*Corresponding author: kwok-fai.chung@polyu.edu.hk

Abstract

In order to enable accurate analysis and prediction on structural behaviour of high strength S690 steel member at large deformations, an integrated experimental, theoretical and numerical investigation to formulate a full range constitutive model is reported in this paper. It is well known that standard tensile tests are effective means to obtain key mechanical properties of coupons for deformations up to on-set of necking. However, owing to non-uniform cross-sectional distributions in both stresses and strains within the necking regions of the coupons, it is important to allow for these effects when analysing measured forces and extensions to give true stresses and strains of the coupons.

The proposed instantaneous area method has been developed and calibrated against test results of a total of 30 standard tensile tests on S690 cylindrical coupons, and it is formulated with key mechanical properties of engineering stress-strain curves readily obtained from these tests. High resolution digital images of the deformed coupons are captured and analysed to obtain instantaneous dimensions of the necking areas. Through theoretical formulation, true stress-strain curves of the coupons after on-set of necking are derived, and modified with numerical correction factors through successive approximations. After normalization on all the corrected true stress-strain curves, a set of formulae to describe the full-range constitutive model for the high strength S690 steels is proposed. Consequently, the proposed model is readily applicable to both analytical and numerical analyses of the high strength S690 steels and their structural members undergoing both small and large deformations up to fracture.

Keywords:

High strength steels; constitutive model; true stress-strain curves; instantaneous dimensions; and non-uniform cross-sectional distributions.

1. Introduction

Owing to recent advances in metallurgy, a wide range of structural steels are readily engineered through alloy design, heat treatment, and mechanical rolling to produce specific crystallized forms which possess different mechanical properties. These include i) Ferritic, ii) High Strength Low Alloy (HSLA), iii) Dual Phase (DP), iv) Transformation Induced Plasticity (TRIP), and v) Martensitic (MS) steels with different deformation characteristics in terms of strength and ductility [1-4]. It should be noted that even though some steels have the same chemical compositions, different continuous controlled cooling processes will lead to different phases (or crystallization forms) which have various combinations of soft-matrix and hard-reinforcement microstructures. Common delivery conditions of these steels are: i) as-rolled condition, ii) normalized condition, iii) thermo-mechanically controlled condition (TMCP), and iv) quenched and tempered condition [5-9]. For American steels, they are supplied to ASTM standards and specifications [10-14], which are equivalent to the European steels with similar manufacturing methods [15-16]. Hence, owing to different delivery conditions, these steels possess very different mechanical properties, and Figure 1 illustrates typical stress-strain curves of these steels according to their steel grades. Unlike normal strength S235 to S460 steels which are traditional pearlitic-ferritic steels, high strength S690 steels to BS EN 10025-6:2005 are martensitic (MS) steels which are produced under a quenched and tempered delivery condition. Hence, they possess very different stress-strain characteristics, when compared with those pearlitic-ferritic steels.

Over the past twenty years, various types of high strength steels, such as S690, S890, and S960, have been produced successfully in many parts of the world. These high strength steels are highly attractive to structural engineers because of their high strength to self-weight ratios. They offer excellent mechanical properties, such as high yield and tensile strengths as well as high toughness, in comparison with those commonly used normal strength steels such as S355 steels. Although they have relatively low tensile to yield strength ratios, and reduced elongation at fracture, the existing design standards and codes of practice [17-22] also accept the high strength steels for structural uses with specific mechanical and ductility requirements. It is generally believed that a wide adoption of these high strength steels will lead to a significant reduction in sizes and self-weights of many structural members, and hence, in overall construction costs.

1.1 Ductility requirements on engineering stress-stress characteristics

According to EN 1993-1-1 [17], various ductility requirements for normal strength S235 to S460 steels are stipulated as follows:

i) the tensile to yield strength ratio, $f_u / f_y \geq 1.10$, 1a)

ii) the limiting strain at fracture, $\varepsilon_L \geq 15\ \%$, and 1b)

iii) the strain corresponding to tensile strength, $\varepsilon_u \geq 15\ f_y / E$. 1c)

For those high strength S690 steels, BS EN 1993-1-12 [18] provides the following modified ductility requirements:

i) the tensile to yield strength ratio, $f_u / f_y \geq 1.05$, 2a)

ii) the limiting strain at fracture, $\varepsilon_L \geq 10\ \%$, and 2b)

iii) the strain corresponding to tensile strength, $\varepsilon_u \geq 15\, f_y / E$. 2c)

In general, these requirements are considered to be rather stringent, in particular, the requirements on the tensile to yield strength ratio and the limiting strain at fracture.

1.2 Standard tensile tests and simplified material models

Standard tensile tests have been widely employed by researchers and engineers in both structural and mechanical engineering to obtain engineering stress-strain curves as well as key mechanical properties of structural steels. These include i) both yield strength f_y and tensile strength f_u , ii) Young's modulus E , iii) a limiting strain at fracture, ε_L , and iv) a strain corresponding to tensile strength, ε_u . These data are used to define engineering stress-strain curves of the steels, and they are readily adopted in structural design and analyses of steel structures.

In general, all standard tensile tests should be conducted in accordance with established testing standards. [23-24]. These standards allow the use of both proportional and non-proportional tensile coupons to examine key mechanical properties of structural steels. However, the values of elongation at fracture for coupons of the same steels but having different gauge lengths are different. This phenomenon is thoroughly presented in the Appendix X1 of ASTM E8/E8M-16 [24] which recommends a rational control using a standard ratio between the gauge length L_o and the cross-sectional area A_o, i.e. L_o / $(A_o)^{0.5}$, for direct comparison. Hence, a proportional specimen should be adopted for a systematic study on the mechanical properties of steel materials. More specifically, according to BS EN ISO 6892-1 [23], the gauge length L_o of proportional coupons is given by $5.65\times\sqrt{A_o}$ where A_o is the nominal cross-sectional area of the coupon, i.e. L_o = 5 d where d is the diameter for a coupon with a circular cross-section.

Conventionally, three simplified constitutive material models of structural steels have been widely adopted for numerical modelling by researchers and engineers [25-29], namely i) an elastic-perfectly plastic model; ii) an elastic-linearly hardening model; and iii) a tri-linear model, as illustrated in Figure 2. It should be noted that

i. The elastic-perfectly plastic model is commonly regarded as a bi-linear material model. For the linear elastic stage, the stress increases linearly with the strain up to the yield strength, f_y . In the perfectly plastic stage, the steel undergoes plastic deformations with the stress being maintained at f_y. This model is widely adopted in many design standards and codes of practice [17-22] for design and analysis of steel structures with small plastic deformations as it always gives conservative structural predictions.

ii. The elastic-linearly hardening model is also a bi-linear material model, which consists of an initial linear elastic stage up to the yield strength f_y , and the subsequent linear strain hardening stage up to the tensile strength, f_u . This model is commonly considered as a typical stress-strain relationship for both annealed steels and normalized steels with improved ductility.

iii. The tri-linear model consists of the following three stages, namely, a) a linear elastic stage,

b) a perfectly plastic stage, and c) a linearly strain hardening stage. This is a typical simplified stress-strain relationship for as-rolled carbon steels and high strength low alloy steels, and it is commonly adopted by researchers and engineers in numerical analyses and design of steel structures.

Other than the above three constitutive models, some researchers [30-31] adopt multi-linear models or even deterministic true stress curves as the constitutive models to assess structural behaviour of structural members and systems. However, these constitutive models are only applicable for deformations up to the on-set of necking. In recent years, researchers of structural engineering conducted their investigations into overall structural behaviour of typical structural members such as beams, columns, and tension braces [31-34] by adopting some advance constitutive material models for deformation ranges up to the on-set of necking. These models are derived by applying conventional transformation rules based on integration method [35,36]. For deformations beyond the on-set of necking, simplified empirical formulae are often adopted to describe their true stress-strain characteristics, and these formulae are commonly known as "Linear Law" and "Power Law" [35-39]. However, owing to lack of test data, and hence, calibration against test data, accuracy of these empirical formulae in predicting true stress-strain responses is somehow uncertain. Thereafter, a modified empirical method, namely "Weighted Average Method" was devised [34-36] to modify these formulae to give improved results. However, this method is not able to provide comprehensive explanations to these corrections.

1.3 Non-uniformity of stress and strain distribution after necking

It is well known [36, 38, 40-42] that a tensile coupon exhibits different mechanical behaviour as it elongates, in particular, i) before on-set of necking, and ii) after on-set of necking. Thus, different methods to determine true stress-strain curves of structural steels should be employed correspondingly. It should be noted that both true stress and true strain refer to the most critical values at the centre of the minimum cross-section because of highly non-linear stresses and strains induced across the minimum cross-section after necking.

In standard tensile tests, both the true stress and the true strain should be determined as follows:

a) Deformations up to on-set of necking:
The true stresses and strains should be determined by applying conventional transformation rules based on integration method [35,36]. All stresses and strains are uniformly distributed over the cross-section within the gauge length. Hence, the true stress and the true strain are always equal to the average stress and the average strain of the cross-section, respectively.

b) Deformations after on-set of necking:
As deformations are highly localized in the necked region, both the stress and the strain vary significantly i) along the longitudinal direction, and ii) over the cross-section, as shown in Figure 3. Hence, the maximum values of the stress and the strains at the centre of the critical (minimum) cross-section should be adopted as the true stress and the true strain respectively. However, these values cannot be measured directly in experiments.

In general, only initial dimensions of steel coupons are measured before testing, and few

attempts are made to measure instantaneous dimensions of the steel coupons, such as the diameter of the critical cross-section, accurately after on-set of necking.

Therefore, it is important to allow for the effect of non-uniformity of stress and strain distribution after necking to obtain a full range constitutive model of structural steels, which is highly desirable for accurate analysis and prediction of structural behaviour of steel structures when these structures or members undergo large deformations up to fracture.

2. Objectives and scope of work

Over the past few years, a comprehensive research programme on scientific investigations into structural performance of high strength S690 steels and welded members is performed by the authors to promote effective use of the S690 steels in construction. In order to enable accurate analysis and prediction on structural behaviour of the S690 steel members at large deformations, there is a need to formulate a full range constitutive model for the S690 steels up to fracture. It is well known that standard tensile tests are effective means to obtain key mechanical properties of coupons for deformations up to on-set of necking. However, owing to non-uniform cross-sectional distributions in both stresses and strains within the necking regions of the coupons, it is important to allow for non-uniform distributions of stresses and strains when analysing measured forces and extensions to give true stresses and strains of the coupons.

This paper presents an integrated experimental, theoretical and numerical investigation for the S690 steels to formulate a full range constitutive model of the S690 steels up to fracture, and the following forms of investigation are conducted:

- Task A Experimental investigations
  A total of 30 standard tensile tests on standardized cylindrical coupons machined from five different S690 steel plates are conducted to provide test data to generate a family of full range engineering stress-strain curves through analyses on high resolution digital photos. Hence, key mechanical properties of the steels, namely, i) both yield strength f_y and tensile strength f_u , ii) Young's modulus E , iii) the limiting strain at fracture, ε_L , iv) the strain corresponding to the tensile strength, ε_u , and more importantly, v) instantaneous deformations, i.e. longitudinal elongations and lateral contraction of the necking areas of the coupons are obtained.

- Task B Theoretical and numerical investigations
  An integrated experimental, theoretical and numerical method proposed by the authors [40-42] for formulation of true stress-strain curves of structural steels is adopted. Based on the key mechanical properties obtained in Task A, full range true stress-strain curves are derived with theoretical formulation, and modified with numerical correction factors through successive approximations. After normalization on all the corrected true stress-strain curves, a set of formulae to describe the full-range constitutive model for the high strength S690 steels is proposed.

Key areas of interest in the present investigation include:

a) deformation characteristics and engineering stress-strain curves of the coupons after on-set

of necking;

b) large deformations in the coupons after necking with varying instantaneous diameters, and hence, non-uniform stress and strain distributions within the necking areas; and
c) formulation of a full range true stress-strain curve for the S690 steels up to fracture based on measured key mechanical properties as well as instantaneous dimensions of the coupons through successive approximations.

Similar to many constitutive models, the proposed model is essentially a rigorously calibrated true stress-strain ($\sigma_t - \varepsilon_t$) curve based on measured engineering stress-strain ($\sigma_e - \varepsilon_e$) curves and instantaneous dimensions of the S690 steel coupons. Hence, accuracy of the proposed model depends heavily on the quality of the measured data: number of tests, precision of tensile tests as well as data measurements and analyses, in particular, in large deformation ranges.

All the coupons are machined from five different S690 steel plates which are purchased in different batches, and Table 1 summarizes typical chemical compositions of these S690 steel plates together with requirements on the corresponding chemical compositions stipulated in EN 10025-6:2004. It is evident that all chemical compositions of these S690 steel plates are well within the maximum limits, especially for Phosphorous (P) and Sulphur (S) which have significant adverse effects onto the mechanical properties of the steel plates. Hence, these S690 steel plates are considered to be representative to common S690 steel plates widely available in the market, and key findings of this investigation are acceptable for general applications.

3. Experimental Investigations using Standard Tensile Tests

A total of 30 standard tensile tests on standardized and proportional cylindrical coupons extracted from both transverse and longitudinal directions of the parent steel plates are carried out, and the test programme is summarized in Table 2. It should be noted that there are a total of 5 series of coupons, namely, Series CA to CE, and in each series, there are 6 coupons to be tested, i.e. 3 coupons are machined along the longitudinal direction of the steel plate, and another 3 coupons along the transverse direction. Typical geometry and dimensions of the cylindrical coupons are shown in Figure 4a). The nominal diameter of the coupons within the gauge lengths is 6.0 mm while the gauge length of all the coupons is taken as 5 d or 30.0 mm. Hence, the relationships between the gauge length and the diameter of the coupons comply with the requirements in BS EN ISO 6892-1 (CEN, 2009).

All the coupons are sampled at the middle of the plate thicknesses, and machined using a high precision Computer Numerical Control (CNC) machine. Figure 4b) illustrates the designation system of these coupons based on section shapes, plate labels, directions of extraction, and serial numbers.

3.1 Test set-up, instrumentation and procedures

A high precision test machine, namely, Testometric CX M500 Testing Machine, is employed to conduct all the tensile tests, as shown in Figure 5. The loading rates in the standard tensile tests are carefully controlled at various deformation stages, as shown in Figure 6a) in accordance with various requirements given in BS EN ISO 6892-1. The values of different

loading rates are summarized in Table 3 while a graphical presentation of the transient strain history during testing is illustrated in Figure 6b). It should be noted that the loading rates adopted in all the tests are kept to be sufficiently slow in order to obtain static values of the mechanical properties of the S690 steels.

In each test, two strain gauges of Model YFLA5 manufactured by Tokyo Sokki Kenkyujo are attached firmly onto the surfaces of the coupon at its mid-length using an adhesive of Model CN-Y in order to measure its elongations accurately in the yielding range. Moreover, in order to capture deformations of the coupon after yielding up to fracture, a non-contact measurement method with digital photo analysis is adopted as follows:

a) the gauge length of the coupon is equally divided with alternate colours into six segments, i.e. 30.0 mm / 6, and thus, each segment is 5.0 mm long;

b) a high resolution digital camera is mounted in front of the test machine, and digital photos of the coupon are taken at close intervals in order to capture incremental deformations of the coupon throughout the test;

c) with a fixed focal distance in each test, all dimensions of the deformed coupon are directly proportional to the numbers of pixels in the digital photos; hence, the axial elongations of each segment within the gauge length as well as the instantaneous diameter of the critical cross-section of the coupon are obtained from counting the numbers of pixels of the deformed coupon in the digital photos taken sequentially.

Hence, both the small deformations of the coupons in the yielding range and the large deformations of the coupons undergoing strain hardening after yielding, through necking and up to fracture have been obtained with high precision.

3.2 Test results

All the standard tensile tests have been conducted successfully according to BS EN ISO 6892-1 (2009) [23] to determine the key mechanical properties of the S690 steels.

3.2.1 Deformations by digital photo analysis

By analysing digital photos of each test, the tensile strains of each segment as well as those of the gauge length ε_e , and the instantaneous diameter, d_i , of the critical (minimum) cross-section of the coupons are readily obtained throughout the entire deformation range of the test. Table 4 illustrates a typical example to determine these values at various deformations. It is shown that:

i) in general, accuracy of the digital photo analysis depends on the measurement set-up and the resolution of the digital photos, and the instantaneous dimensions are obtained according to the following:

= 30.0 / 2160 = 0.0139 mm / pixel for length measurement
= 6.0 / 410 = 0.0146 mm / pixel for diameter measurement

ii) under yield condition, the strains of these six segments vary from 0.00 to 1.16 % while the

average strain ε_i is 0.45 %, which is larger than the value measured by the strain gauges at 0.36 %;

ii) under necking condition, the strains of these six segments are shown to be fairly uniform as they vary narrowly from 6.30 to 6.65 %, while the average strain ε_i is 6.48 %; this agrees very well with the value measured by the strain gauges at 6.49 %;

iii) under fracture condition, the strains of these six segments vary significantly as they range from 5.67 to 69.04 %, and it should be noted that a highly localized necking occurs within Segment No. 5;

iv) since the axial deformations before and up to the yield condition are rather small, the change in length in term of the number of pixels is correspondingly small, leading to some errors, and hence, the strains measured with the strain gauges should be used; and

v) reduction in diameter of the critical (minimum) cross-sectional area after yielding becomes apparent, and hence, the corresponding changes in the number of pixels from the yielding condition to the facture condition are readily determined to give accurate values of the instantaneous diameter, d_i.

Typical full range engineering stress-strain (σ_e - ε_e) curves of the tensile test is plotted in Figure 7a) while the (d_i - ε_e) relationship is shown in Figure 7b). It should be noted that the (d_i - ε_e) relationship provides an important means to determine the instantaneous area, A_i , to evaluate a) average true stress, and b) true strain of the critical cross-section of the coupon, as described in in Section 4.1. Figure 8 shows a typical fracture surface of the steel coupon after testing, showing tensile fracture in the central core and shear fracture in the surrounding materials of the coupon.

3.2.2 Key mechanical properties

After a comprehensive data analysis on all these digital photos as described above, Figure 9 plots all the derived engineering stress-strain (σ_e - ε_e) curves of each of the five test series of the high strength S690 steels onto the same graph for direct comparison. It is shown that all of these curves in Figures 9a) to 9e) are very similar to each other throughout the entire deformation ranges of the tests. Figure 9f) plots all these 30 curves onto the same graph to demonstrate consistency of their deformation characteristics.

Table 5 summarizes key mechanical properties of all the coupons in the five test series. In general, the values of many quantities such as the yield strength f_y , the tensile strength f_u and the strain at fracture ε_L within a test series are very similar to one another, and both their standard derivations and coefficients of variation are shown to be very small. It is found that:

a) The average yield strengths f_y among the five series range from 731 to 801 N/mm^2 while the corresponding average tensile strengths f_u range from 769 to 851 N/mm^2. Moreover, the corresponding tensile to yield strength ratios f_u / f_y of the five series range from 1.05 to 1.06.

b) The minimum values of the strains at fracture, ε_L , in each series of the five test series range from 15.6 to 17.3 %, i.e. they are significantly larger than 10%.

c) The minimum values of the strains corresponding to the tensile strength, ε_u , in each series of the five test series range from 5.1 to 6.5 %, and they are shown to be larger than the corresponding values of 15 f_y / E_s .

Consequently, the steels are demonstrated to meet all ductility requirements stipulated in BS EN 1993-1-12. Moreover, the basic mechanical properties of these engineering stress-strain curves are shown to have significant variations among themselves, and they may be readily considered to be representative to a wide range of common S690 steel plates. This allows key findings of this investigation to be acceptable for general applications.

4. Theoretical and Numerical Investigations

An integrated experimental, theoretical and numerical method proposed by the authors [40-42] is adopted for formulation of true stress-strain curves of structural steels. Based on the key mechanical properties obtained in Task A, full range true stress-strain ($\sigma_t - \varepsilon_t$) curves are derived with theoretical formulation, and modified with numerical correction factors through successive approximations. After normalization on all the corrected true stress-strain curves, a set of formulae is proposed to describe the full-range constitutive model for the high strength S690 steels.

4.1 Formulation of true stress-strain curves

In order to describe the deformation characteristics of the S690 steels in both small and large deformations with a high accuracy, the following two methods are adopted to describe different deformation ranges of the proposed material model:

c) Deformations up to on-set of necking: Integration method

This is a simple and well established analytical method derived from integrating strains of a deformed steel coupon, and it is assumed that the volume of the steel remains constant during deformations. Hence, the true stress σ_t and the true strain ε_t of the coupon up to on-set of necking are given by:

$$\varepsilon_t = \ln\ (1 + \varepsilon_e) \quad \text{3a)}$$

$$\sigma_t = \sigma_e\ (1 + \varepsilon_e) \quad \text{3b)}$$

where σ_e and ε_e are the engineering stress and the engineering strain respectively; and
σ_t and ε_t are the true stress and the true strain respectively.

b) Deformations after on-set of necking: Instantaneous area method

Based on the assumption of constant volume in the coupon undergoing large deformations, both the true stress σ_t and the true strain ε_t of the coupon after on-set of necking are given by:

$$\varepsilon_t = \eta_\varepsilon\ ln\left({A_o}/{A_i}\right) \quad \text{4a)}$$

$$\sigma_t = \eta_\sigma\ \ {N_i}/{A_i} \quad \text{4b)}$$

where A_o is the original cross-sectional area ;
A_i is the measured instantaneous cross-sectional area under applied load N_i ;
η_ε is a correction factor due to a non-uniform strain distribution within the critical (minimum) cross-section of the coupon ; and
η_σ is a correction factor due to a non-uniform stress distribution within

the critical (minimum) cross-section of the coupon.

It should be noted that the values of both η_ε and η_σ may be taken as 1.0 initially, and each of them will converge to certain values after successive approximations through numerical modelling as described in Section 4.2.

Through the use of the instantaneous diameter d_i of the coupon obtained from the digital photo analysis described in Section 3.2.1, the values of A_i are readily obtained, and hence, both the true stress σ_t and the true strain ε_t are determined with Equations. 4a) and 4b). Hence, the entire true stress-strain (σ_t - ε_t) curve of the coupon may be obtained with both the measured engineering stress-strain (σ_e - ε_e) curve and the instantaneous cross-sectional area A_i of the coupon. This true stress-strain curve is generally considered to be the first approximation to the accurate curve, i.e. the predicted true stress-strain (σ_t - ε_t) curve (first approximation), and non-uniform distributions in both the stresses and the strains of the critical (minimum) cross-section after on-set of necking should be allowed for as described in the next section.

4.2 Successive approximations through numerical modelling

In order to improve accuracy of this predicted true stress-strain curve, an advanced finite element model of the tensile test is established to simulate deformation characteristics of the coupon. This provides a predicted load-extension $(N - \delta)_p$ curve of the tensile test together with various stress-strain plots across the critical cross-section of the coupon under various deformation stages. Due to these non-uniform stress and strain distributions, the following two correction factors of the critical cross-section are established, and they are defined as follows:

$$\text{Stress correction factor, } \eta_\sigma = \frac{\sigma_{vm,max}}{\sigma_{av}} \qquad 5a)$$

$$\text{Strain correction factor, } \eta_\varepsilon = \frac{\varepsilon_{p,max}}{\varepsilon_{av}} \qquad 5b)$$

where $\sigma_{vm,max}$ is the maximum von Mises stress of the critical cross-section;
σ_{av} is the average direct stress across the critical cross-section;
$\varepsilon_{p,max}$ is the maximum principal true strain of the critical cross-section; and
ε_{av} is the average direct strain across the critical cross-section.

After working out the values of both η_σ and η_ε according to Equation 5, the predicted true stress-strain (σ_t - ε_t) curve is then updated according to Equation 4 for prediction of an improved load-extension $(N - \delta)_p$ curve as well as an improved distribution of stress and strain in the coupon after necking. By repeating the process until convergence of the correction factors, η_σ and η_ε, is achieved, the updated true stress-strain (σ_t - ε_t) curve of the coupon is hence established. Figure 10 illustrates the entire process of the proposed instantaneous area method in deriving the true stress-strain (σ_t - ε_t) curve using numerical correction factors η_σ and η_ε through successive approximations in a flow chart.

4.3 An illustrative example

An example of the proposed instantaneous area method on the deformation characteristics of

the S690 steel is described as follows:

Coupon CC-T03 is taken as an example. Both the engineering stress-strain (σ_e - ε_e) curve obtained from Task A after digital photo analysis and the true stress-strain (σ_t - ε_t) curve derived using Equations 4 and 5 are plotted in the same graph as illustrated in Figure 11. Moreover, the true stress-strain (σ_t - ε_t) curves derived with both the Linear Law and the Power Law are presented for easy comparison.

In order to improve accuracy of the predicted true stress-strain curve, a non-linear finite element model using ABAQUS 6.13 [43] is established to simulate the tensile test, and an eight-noded solid element with reduced integration, C3D8R, is adopted to model the coupon. Figure 12 shows the finite element mesh under longitudinal tension, and local refinement with an element size of 0.3 x 0.3 x 0.3 mm is adopted near the middle of the gauge length of the coupon. For details of the finite element modelling technique including i) mesh configurations with local refinement, ii) convergence study on various mesh configurations and element sizes, and iii) numerical accuracy of the finite element models, refer to Ho et al. [42]. Both the measured and the predicted load-extension (N – δ) curves are plotted onto the same graph in Figure 13 for direct comparison. It is shown that

a) the predicted load-extension $(N - \delta)_p$ curves obtained with the finite element model using the predicted true stress-strain $(\sigma_t - \varepsilon_t)_p$ curves based on both Linear Law and Power Law do not provide satisfactory results; and

b) more interestingly, the predicted load-extension $(N - \delta)_p$ curve obtained with the finite element model based on the predicted true stress-strain $(\sigma_t - \varepsilon_t)_p$ curve (first approximation) does not give a good prediction as well.

A detailed investigation into the cross-sectional stress-strain distributions at the critical (minimum) cross-section of the finite element model shows that highly non-uniform stress and strain distributions occur across the minimum cross-section of the coupon after necking. Figure 14a) presents the cross-sectional stress distributions of both $\sigma_{vm,max}$ and σ_{av} within the critical cross-sections at various deformations obtained in the first approximation. After determining the values of both correction factors η_σ and η_ε , an updated true stress-strain (σ_t – ε_t) curve of the coupon is obtained, as shown in Figure 15a). This updated curve is incorporated into the finite element model to generate an updated load-extension $(N - \delta)_p$ curve, as shown in Figure 15b). It is evident that by incorporating the updated true stress-strain (σ_t – ε_t) curve, an improved prediction to the load extension $(N - \delta)_p$ curve of the tensile test is achieved. By re-evaluating the values of both η_σ and η_ε , and hence, updating the finite element model, improvements to the true stress-strain (σ_t – ε_t) curve, and hence, the load-extension $(N - \delta)_p$ curves are achieved.

Table 6 summarizes the values of various stress and strain correction factors, η_σ and η_ε , to the true stress-strain (σ_t – ε_t) curves at various deformations through successive approximations. It should be noted that this process of successive approximation repeats until the values of both η_σ and η_ε at various deformations become converged, i.e. the difference in the values of both

η_σ and η_ε in two successive approximations is smaller than a pre-determined tolerance which is commonly taken to be 0.01. It is shown in Table 6 that after 5 successive approximations, the values of both η_σ and η_ε have converged, and the corresponding stress distributions of both $\sigma_{vm,max}$ and σ_{av} are plotted in Figure 14b) for easy comparison. Both the predicted true stress-strain $(\sigma_t - \varepsilon_t)_p$ curves and the predicted load-extension $(N - \delta)_p$ curves derived at various approximations are plotted in Figure 15 for direct comparison with the measured results. Hence, a corrected full range true stress-strain $(\sigma_t - \varepsilon_t)$ curve for the S690 coupon is established and calibrated successfully against the test data of the tensile test throughout the entire deformation range.

It should be noted that the proposed method has been employed to derive a specific true stress-strain $(\sigma_t - \varepsilon_t)_p$ curve of each of the 30 coupon tests using numerical correction factors through successive approximations. The predicted load-extension $(N - \delta)_p$ curves are found to agree very well with the measured load-extension $(N - \delta)_m$ curves after 4 to 6 approximations in all cases.

5 Proposed constitutive model

In order to generate data to formulate a constitutive model for the S690 steels, both the true stress σ_t and the true strain ε_t of the full range true stress-strain $(\sigma_t - \varepsilon_t)$ curve of each of the 30 coupon tests are normalized to facilitate direct comparison as follows:

$$\text{Normalized true strain ratio, } \varepsilon_{nt} = \quad \varepsilon_t \ E \ / \ f_y \qquad 6a)$$

$$\text{Normalized true stress ratio, } \sigma_{nt} = \quad \sigma_t \ / \ f_y \qquad 6b)$$

All normalized true stress-strain $(\sigma_{nt} - \varepsilon_{nt})$ curves are plotted onto the same graph in Figure 16 for direct comparison, and it is evident that these curves follow each other closely over the entire deformation range. It should be noted that:

a) Figure 16a) illustrates a highly consistent constitutive model for a normalized true strain ε_{nt} up to 18, i.e. approximately up to on-set of necking in the coupons; and

b) Figure 16b) illustrates a consistent constitutive model for a normalized true strain ε_{nt} up to 330, i.e. approximately up to fracture in the coupons.

After data analysis on various parameters of the 30 normalized stress-strain $(\sigma_{nt} - \varepsilon_{nt})$ curves, the following set of formulae is proposed to describe the full range constitutive model of the high strength S690 steels:

$$\sigma_{nt}(\varepsilon)\begin{cases}\sigma_{nt}=\varepsilon_{nt} & \text{for} \quad \varepsilon_{nt}\le 1\\ \sigma_{nt}=1.0+0.003\ (\varepsilon_{nt}-1) & \text{for} \quad 1<\varepsilon_{nt}\le 6\\ \sigma_{nt}=0.91+0.0212\varepsilon_{nt}-0.000625{\varepsilon_{nt}}^{2} & \text{for} \quad 6<\varepsilon_{nt}\le 18\\ \sigma_{nt}=1.09+0.0012\times(\varepsilon_{nt}-18) & \text{for} \quad 18<\varepsilon_{nt}\le 80\\ \sigma_{nt}=1.165+0.0011\times(\varepsilon_{nt}-80) & \text{for} \quad 80<\varepsilon_{nt}\le 330\end{cases} \tag{10}$$

The proposed constitutive model is also plotted in Figure 16 for direct comparison with all the normalized true stress-strain ($\sigma_{nt} - \varepsilon_{nt}$) curves obtained. Comparison shows that the proposed constitutive model is highly effective as a lower bound to describe the true stress-strain characteristics of the high strength S690 steels, and it may be adopted for advanced structural analysis of the high strength S690 steel members.

In order to demonstrate effectiveness of the proposed constitutive model given in Equation 10, the model is adopted in the finite element analysis for Coupon CC.T-03, i.e. the illustrative example presented in Section 4.3. The predicted load-extension $(N - \delta)_p$ curve is plotted in Figure 17 together with the predicted load–extension $(N - \delta)_p$ curve after 5 successive approximations, and also the measured load-extension $(N - \delta)_m$ curve for direct comparison. It is shown that both the predicted $(N - \delta)_p$ curves follow closely to the measured load-extension $(N - \delta)_m$ curve along the entire deformation range. Owing to the successful formulation of the proposed constitutive model, no successive approximation is needed.

6. Conclusions

This paper reports an integrated experimental, theoretical and numerical investigation to formulate a full range constitutive model for accurate analysis and prediction on structural behaviour of high strength S690 steel members. It is well known that standard tensile tests are effective means to obtain key mechanical properties of coupons for deformations up to on-set of necking. However, owing to non-uniform cross-sectional distributions in both stresses and strains within the necking areas of the coupons, it is important to allow for non-uniform distributions of stresses and strains when analysing measured forces and extensions to give true stresses and strains of the coupons.

The proposed instantaneous area method has been developed and calibrated against test results of a total of 30 standard tensile tests on S690 cylindrical coupons, and it is formulated with key mechanical properties of engineering stress-strain curves together with instantaneous dimensions readily obtained in the tests. Through theoretical formulation, true stress-strain curves of the coupons after on-set of necking are derived, and modified with numerical correction factors through successive approximations.

Based on the findings of the integrated experimental, analytical and numerical investigations, it is concluded that:

- Despite a small reduction in ductility with an increase in yield strengths, all the coupons of

the S690 steel plates are found to be able to satisfy the ductility requirements stipulated in EN 1993-1-1 and -12.

- The proposed instantaneous area method is very effective in deriving full range true stress-strain ($\sigma_t - \varepsilon_t$) curves of structural steels, and this method has been successfully applied to derive 30 different full range true stress-strain ($\sigma_t - \varepsilon_t$) curves based on the test results of 30 standard tensile tests on cylindrical coupons machined from five different S690 steel plates.

- After normalization on all the corrected true stress-strain ($\sigma_t - \varepsilon_t$) curves, a set of formulae defining the normalized true stress-strain ($\sigma_{nt} - \varepsilon_{nt}$) curve to describe the full-range constitutive model for the high strength S690 steels is proposed.

Consequently, the proposed constitutive model is readily applicable to both analytical and numerical analyses of the high strength S690 steels and their structural members undergoing both small and large deformations up to fracture.

Acknowledgement

The authors are grateful to the financial support provided by the Research Grant Council of the Government of Hong Kong SAR (Project Nos. PolyU 1526871/16E, 152231/17E and 152157/18E). The project leading to the publication of this paper is also partially funded by the Research Committee (Project Nos. RUQV and RJKB) and the Chinese National Engineering Research Centre for Steel Construction (Hong Kong Branch) (Project No. 1-BBY3 & 6) of the Hong Kong Polytechnic University under the financial support of the Innovation and Technology Commission of the Government of Hong Kong SAR. The research studentships of the second and the fourth authors provided by the Hong Kong Polytechnic University are acknowledged. Special thanks go to the Nanjing Iron and Steel Company Ltd. in Nanjing, the Pristine Steel Fabrication Company Ltd. in Dongguan, and the Industrial Centre of the Hong Kong Polytechnic University. All structural tests on high strength S690 steel materials were carried out at the Structural Engineering Research Laboratory of the Department of Civil and Environmental Engineering at the Hong Kong Polytechnic University, and supports from the technicians are gratefully acknowledged.

REFERENCES

[1] Dieter G.E. Jr. (1961). Mechanical Metallurgy. McGraw-Hill Book Company. New York, U.S.A.

[2] Willms R. (2009). “High strength steel for steel constructions”. Nordic Steel.

[3] Keeler S, and Kimchi M. (2014). Advanced High-Strength Steels Application Guidelines Version 5.0. World Auto Steel, World Steel Association. Brussels, Belgium.

[4] Tasan C.C., Dieh M., Yan D., Bechtold M., Roters F., Schemmann L., Zheng C., Peranio N., Ponge D., Koyama M., Tsuzaki K., and Raabe D. (2015). “An overview of Dual-Phase Steels: Advances in micro-structure-oriented processing and micromechanically guided design”. Annu. Rev. Mater. Res., 2015, 45:391-431.

[5] BS EN 10025-1: 2004. Hot rolled products of structural steels – Part 1: General technical delivery conditions. British Standards Institution.
[6] BS EN 10025-2: 2004. Hot rolled products of structural steels – Part 1: Technical delivery conditions for non-alloy structural steels. British Standards Institution.
[7] BS EN 10025-3: 2004. Hot rolled products of structural steels – Part 1: Technical delivery conditions for normalized/normalized rolled weldable fine grain structural steels. British Standards Institution.
[8] BS EN 10025-4: 2004. Hot rolled products of structural steels – Part 1: Technical delivery conditions for thermomechanical rolled weldable fine grain structural steels. British Standards Institution.
[9] BS EN 10025-6: 2004. Hot rolled products of structural steels – Part 1: Technical delivery conditions for flat products of high strength structural steels in the quenched and tempered condition. British Standards Institution.
[10] ASTM A36/A36M-12. Standard specifications for carbon structural steel. ASTM International, 100 Barr Harbor Drive, PO Box C700, West Conshohockem, PA.
[11] ASTM A514/A514M-18e1. Standard Specification for High-Yield-Strength, Quenched and Tempered Alloy Steel Plate, Suitable for Welding. ASTM International, 100 Barr Harbor Drive, PO Box C700, West Conshohocken, PA.
[12] ASTM A572/A572M-18. Standard specifications for high-strength low-alloy Columbium-Vanadium structural steel. ASTM International, 100 Barr Harbor Drive, PO Box C700, West Conshohocken, PA.
[13] ASTM A709/A709M-18. Standard specifications for structural steel for bridges. ASTM International, 100 Barr Harbor Drive, PO Box C700, West Conshohocken, PA.
[14] ASTM A1066/ A1066M-11. Standard specifications for high-strength low-alloy structural steel plates produced by Thermo-Mechanical Controlled Process (TMCP). ASTM International, 100 Barr Harbor Drive, PO Box C700, West Conshohocken, PA.
[15] Bjorhovde R and Engestrom M. (2001). Structural Steel Selection Considerations: A Guide for Students, Educators, Designers and Builders. American Society of Civil Engineers, Reston, United States.
[16] Chung KF, Chiew SP, and Lee HY. (2015). Professional Guide HKCMSA-P001: Selection of Equivalent Steel Materials to European Steel Materials Specifications. Hong Kong Constructional Metal Structures Association, Hong Kong SAR.
[17] BS EN 1993-1-1 (2005). Design of Steel Structures – Part 1-1: General rules and rules for buildings. British Standards Institution.
[18] BS EN 1993-1-12 (2007). Design of Steel Structures – Part 1-12: Additional rules for the extension of EN 1993 up to steel grades S700. British Standards Institution.
[19] Code of practice for the structural use of steel 2011, Buildings Department, the Government of Hong Kong SAR, October 2011.
[20] Load and Resistance Factor Design Specification for Structural Steel Buildings, American Institute of Steel Construction, Inc., Chicago, IL, December 1999.
[21] ANSI/AISC 360-16. Specification for Structural Steel Buildings, American Institute of Steel Construction, Inc., Chicago, IL, July 2016.
[22] AS4100-1998 (R2016). Steel Structures. Standards Australia, June 1998.

[23] BS EN ISO 6892-1 (2009). Metallic materials – Tensile testing Part 1: Method of test at room temperature. International Organization for Standardization.
[24] ASTM E8/E8M-16. Standard test methods for tension testing for metallic materials. ASTM International, 100 Barr Harbor Drive, PO Box C700, West Conshohockem, PA.
[25] Chiew S.P., Jin Y.F., and Lee C.K. (2016). Residual stress distribution of roller bending of steel rectangular structural hollow sections. *Journal of Constructional Steel Research*, 119: 85-97.
[26] Ban H.Y. and Shi G. (2018). Overall buckling behaviour and design of high-strength steel welded section columns. *Journal of Constructional Steel Research*, 143: 180-195.
[27] Bradford M.A., and Liu X. (2016). Flexural torsional buckling of high-strength steel beams, *Journal of Constructional Steel Research*, 124: 122-131.
[28] Zhao M.S., Lee C.K. and Chiew S.P. (2016). Tensile behavior of high performance structural steel T-stub joints, *Journal of Constructional Steel Research*, 122: 316-325.
[29] Yun X. and Gardner L. (2017). Stress-strain curves for hot-rolled steels. *Journal of Constructional Steel Research*, 133: 36-46.
[30] Green P.S., Sause R. and Ricles J.M. (2002). Strength and ductility of HPS flexural members. *Journal of Constructional Steel Research*, 58: 907-941.
[31] Gardner L., Yun, X., Fieber A., and Macorini L. (2019). Steel design by advanced analysis: material modeling and strain limits. *Engineering*, 5(2): 243-249.
[32] Quach W. M., Teng J. G., and Chung K. F. (2008). Three-Stage Full-Range Stress-Strain Model for Stainless Steels. *Journal of Structural Engineering*, 134(9): 1518-1527.
[33] Tao Z. and Rasmussen K.J. (2008). Stress-strain model for ferritic stainless steel. *Journal of Materials in Civil Engineering*, 28(2): 06015009.
[34] Green P.S. and Varma A.H. (2018). A new stress-strain material model for ductile steels in numerical analysis – a rational approach. *In.: Eighth International Conference on Thin-Walled Structures – ICTWS 2018*, 24~27 July 2018, Lisbon, Portugal.
[35] Ling Y. (1996). Uniaxial true stress-strain after necking. *AMP Journal of Technology*, 5, 37-48.
[36] Roylance D. "Stress-Strain Curves." Massachusetts Institute of Technology Study, Cambridge, 2001.
[37] Jia L.J. and Kuwamura H. (2014). Ductile fracture simulation of structural steels under monotonic tension. *Journal of Structural Engineering, 140*(5): 04013115.
[38] Bridgeman P.W. (1952). Studies in Large Plastic Flow and Fracture, McGraw-Hill, New York, U.S.A.
[39] Zhang K.S. and Li Z.H. (1994). Numerical analysis of the stress-strain curve and fracture initiation for ductile material, *Engng. Fracture Mech.*, 49:235-241.
[40] Ho HC, Liu X, Chung KF, Xiao M. Tensile tests on high strength steel materials with high precision measurements. *In: Fifteenth East Asia-Pacific Conference on Structural Engineering and Construction (EASEC-15)*, 11 ~ 13 October 2017, Xi'an, China. (Paper No.: P1404); 2017.
[41] Ho HC, Liu X, and Chung KF, Xiao M, Yam MCH and Nethercot DA. (2018). True stress-strain characteristics of high strength S690 steels. *International Conference on Engineering Research and Practice for Steel Construction 2018*, Hong Kong, pp 160-167.

[42] Ho HC, Chung KF, Liu X, Xiao M and DA. Nethercot. (2019). Modelling tensile tests on high strength S690 steel materials undergoing large deformations. *Engineering Structures*, 192:305-322.

[43] Abaqus User's Manual. Version 6.13-4. Dassault Systèmes Corp. Providence, RI, USA; 2013.

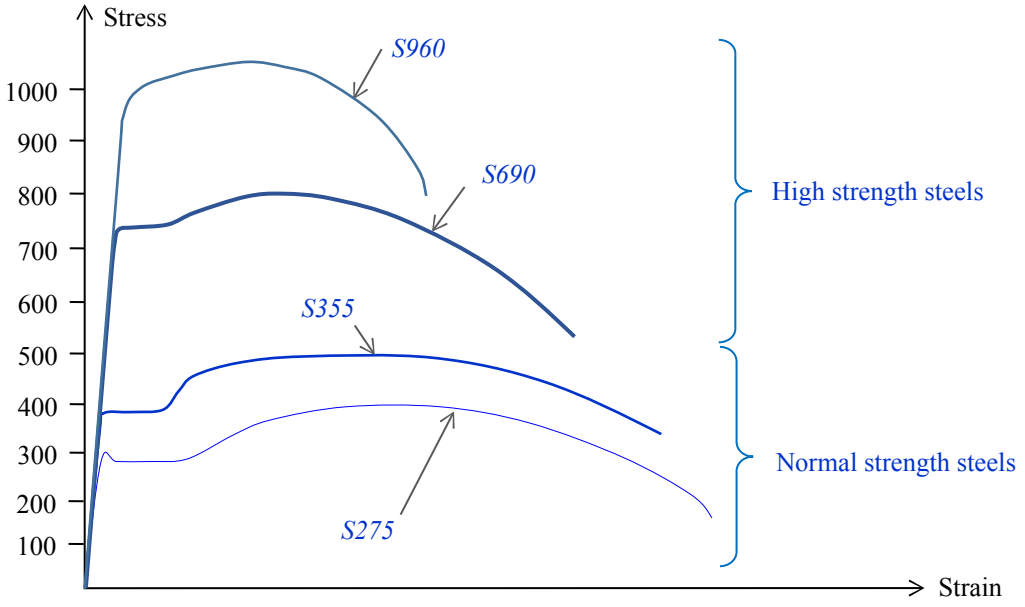

Figure 1 Typical engineering stress-strain curves

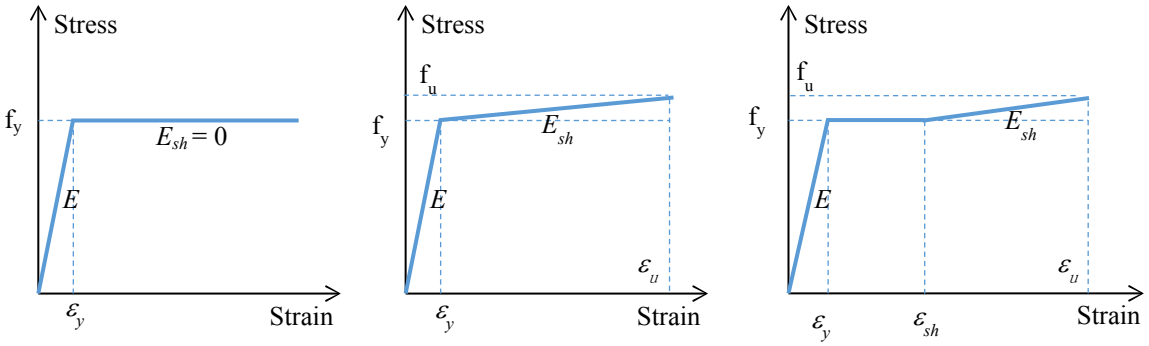

Figure 2 Simplified constitutive models for steels

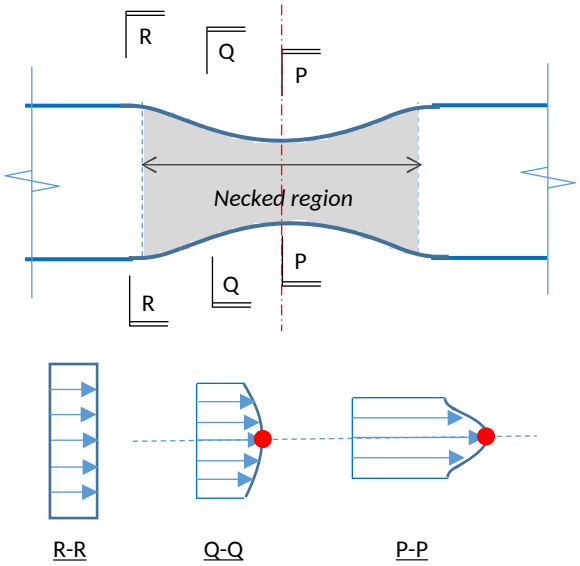

Figure 3 Typical non-uniform distribution in stresses and strains in various cross-sections after necking

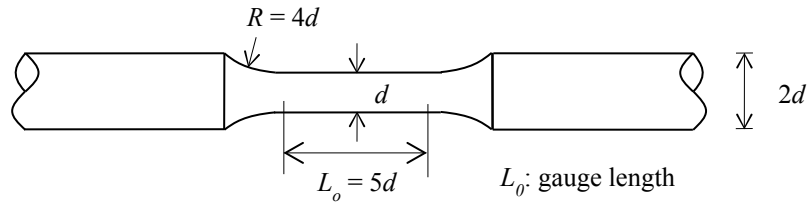

a) Standard cylindrical specimen

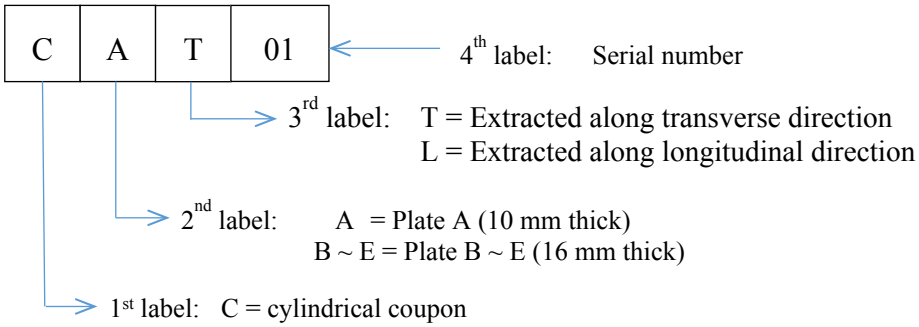

b) Designation system of tensile coupons

Figure 4. Geometry and dimensions of test coupons for monotonic tensile tests

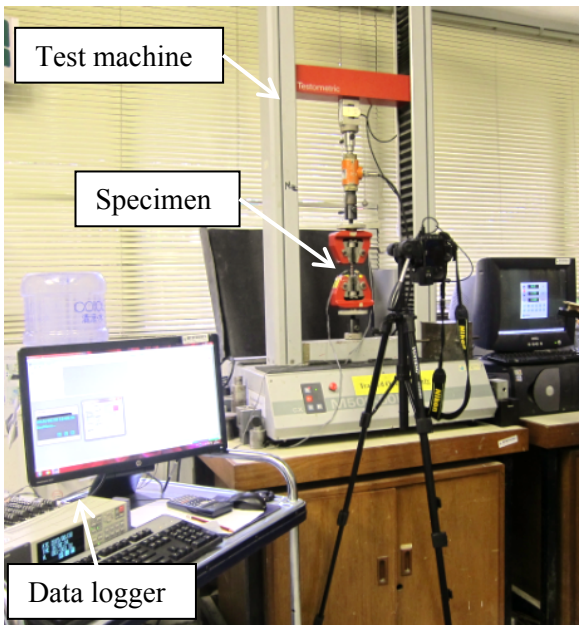

Figure 5. Set-up and instrumentation for monotonic tensile tests

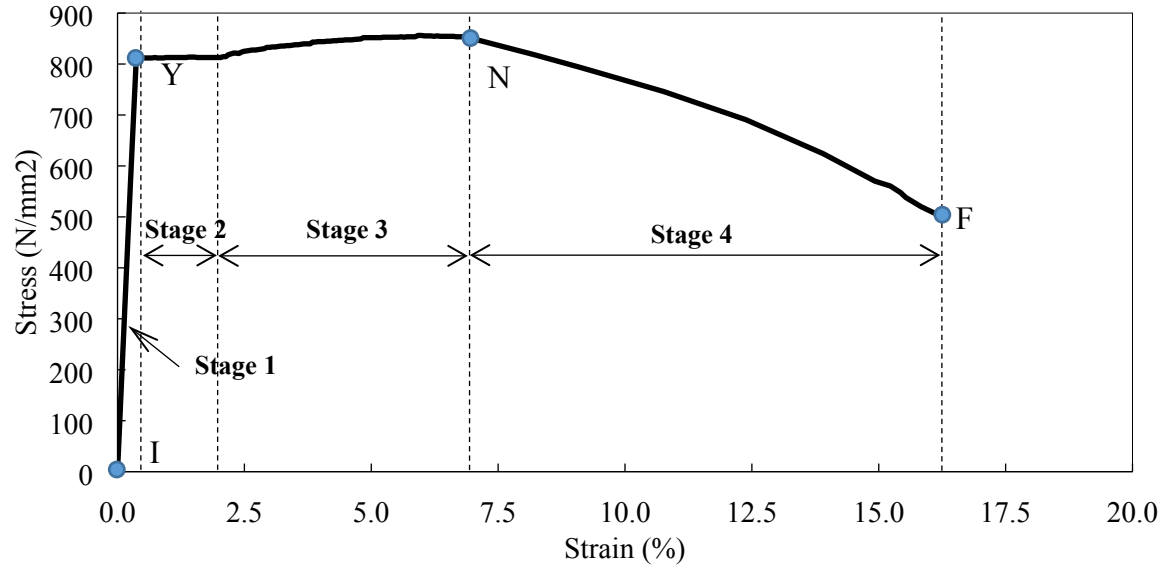

a) Typical stress-strain curve

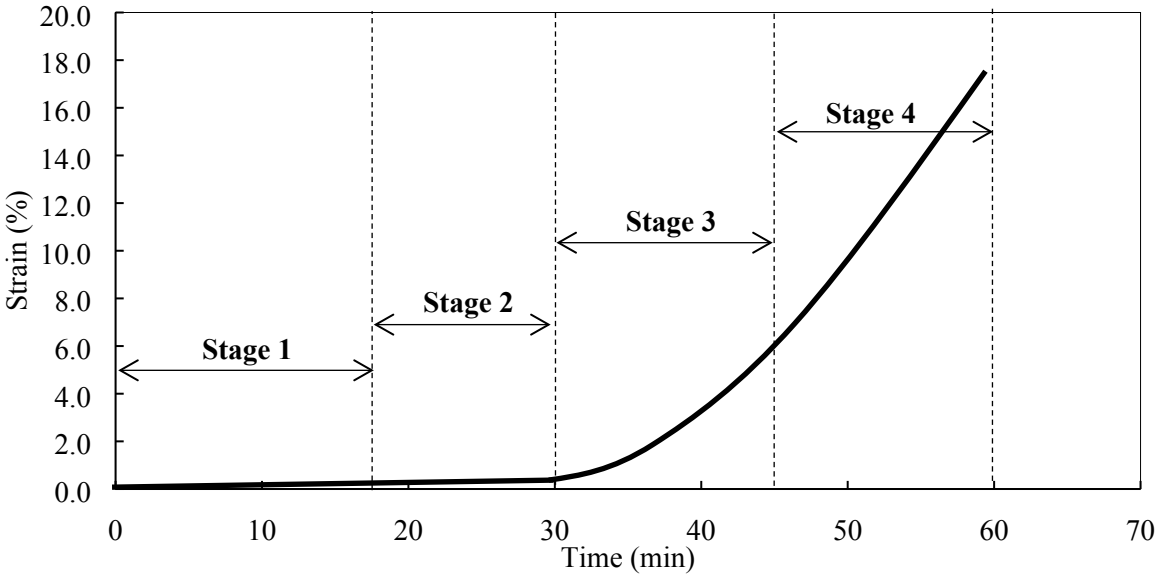

b) Typical transient strain history during testing

Figure 6. Loading rates at various stages of testing

Notes: Stage 1: Linearly elastic stage for determination of Young's modulus
Stage 2: Yield plateau stage for determination of yield strength
Stage 3: Non-linear stage for determination of tensile strength
Stage 4: Non-linear stage for determination of fracture

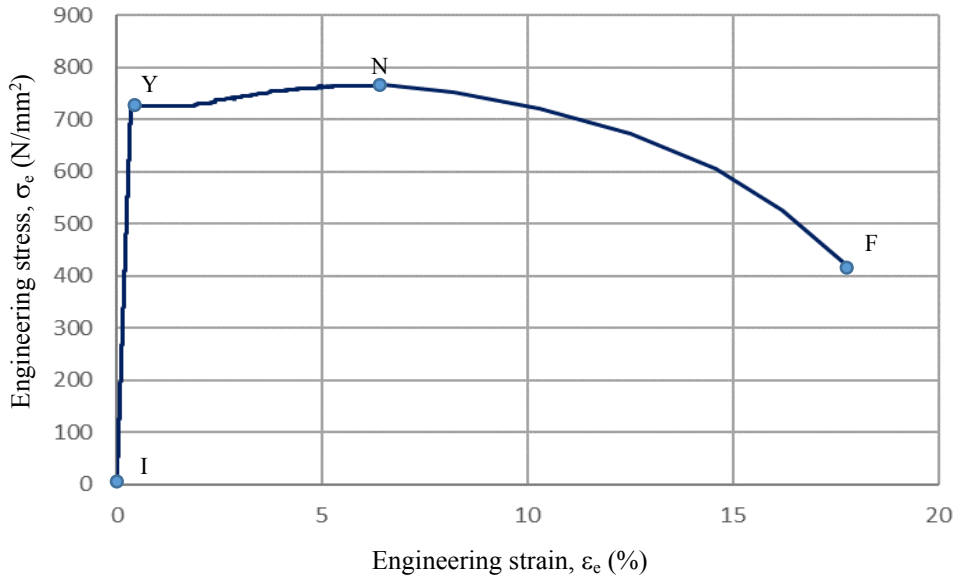

a) Engineering stress strain curve of a typical tensile test

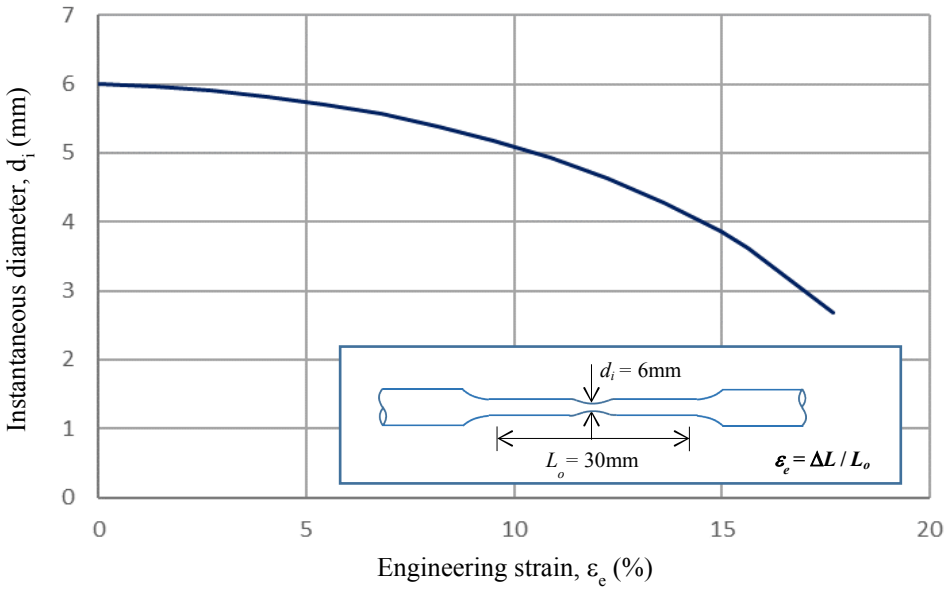

b) Variation of instantaneous diameter against engineering strain

Figure 7 Test results of a typical tensile test

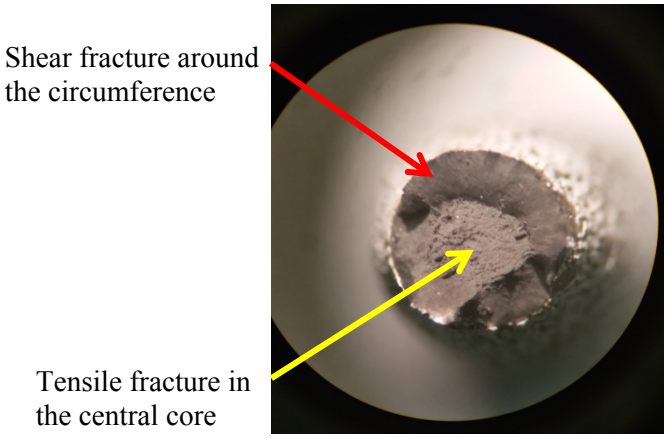

Figure 8. Typical cross-section after fracture

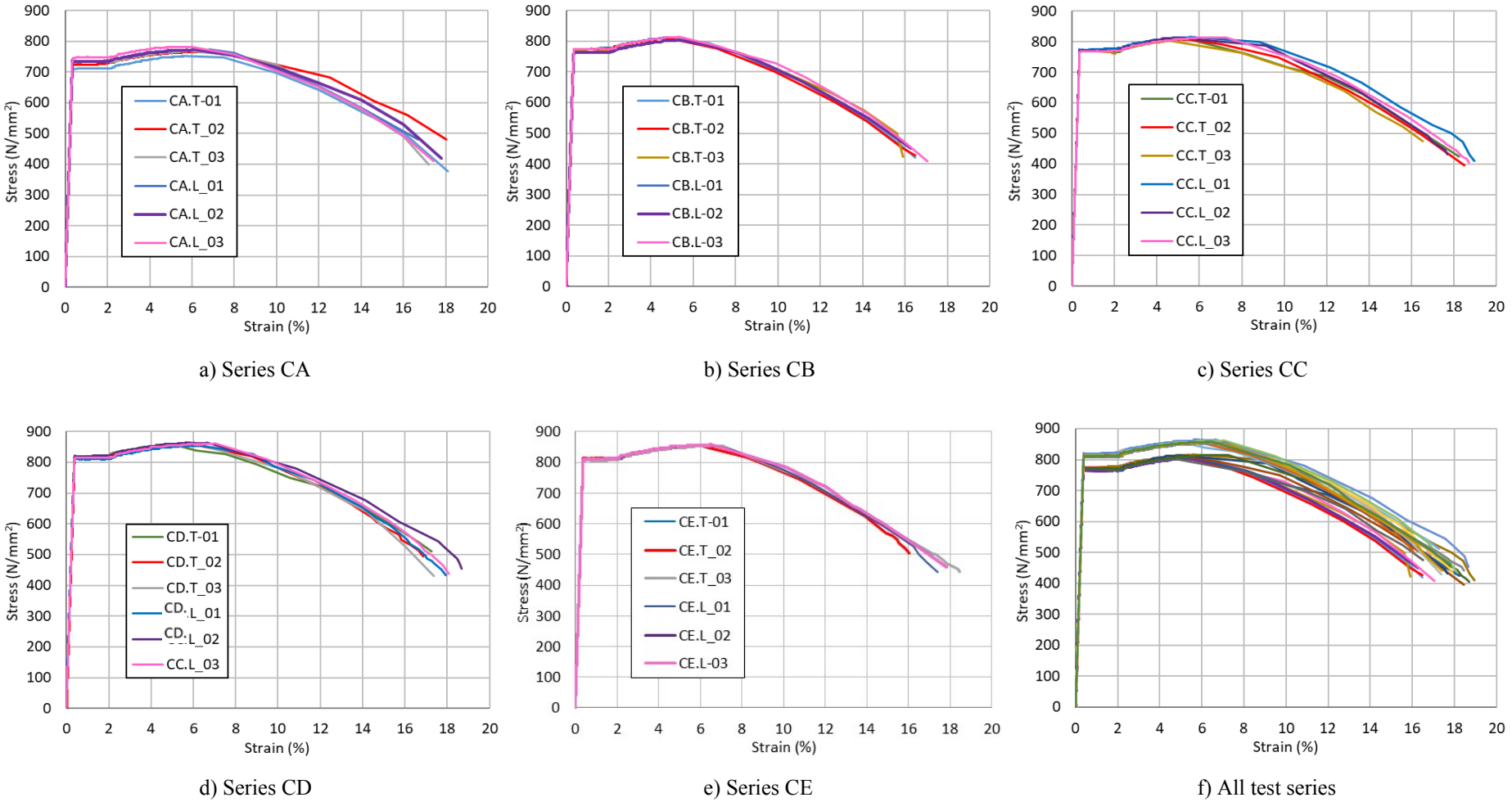

a) Series CA b) Series CB c) Series CC

d) Series CD e) Series CE f) All test series

Figure 9. Engineering stress strain (σ_e - ε_e) curves of tensile coupons

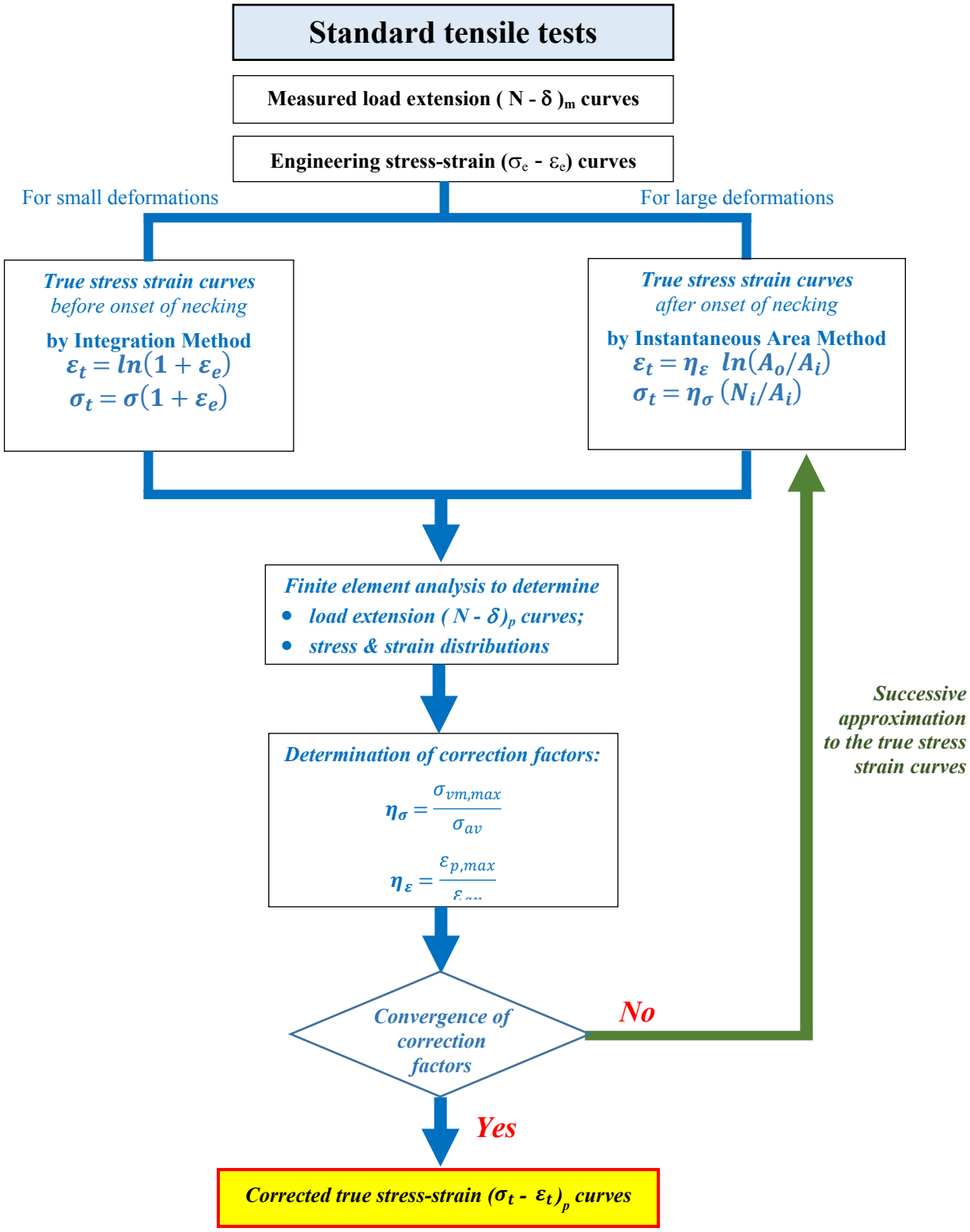

Figure 10. Flow chart of the proposed Instantaneous Area Method with numerical correction factors through successive approximations

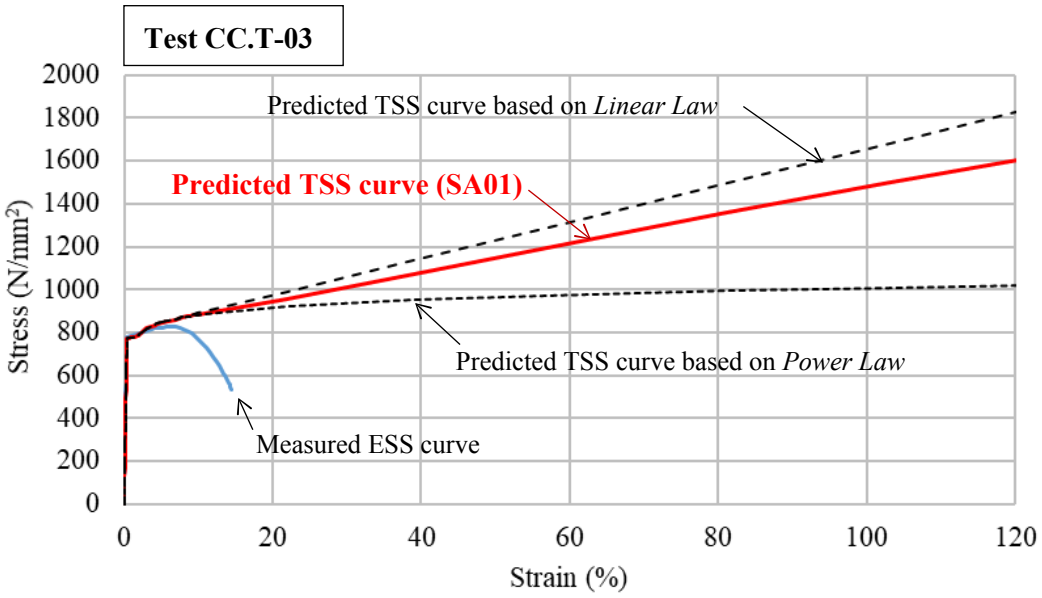

Figure 11: Various stress-strain curves of a S690 tensile coupon test

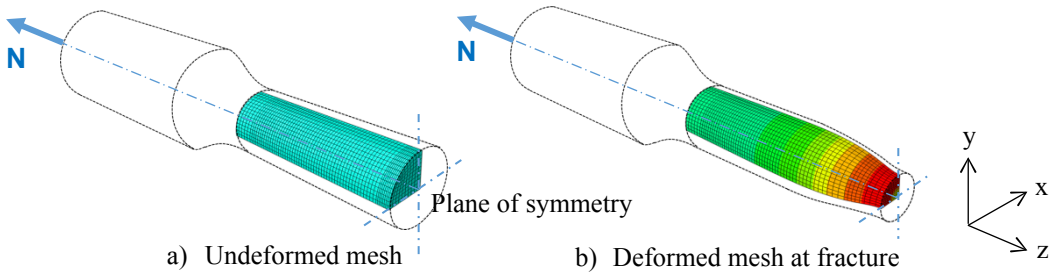

Figure 12: Finite element modelling of a S690 tensile coupon test

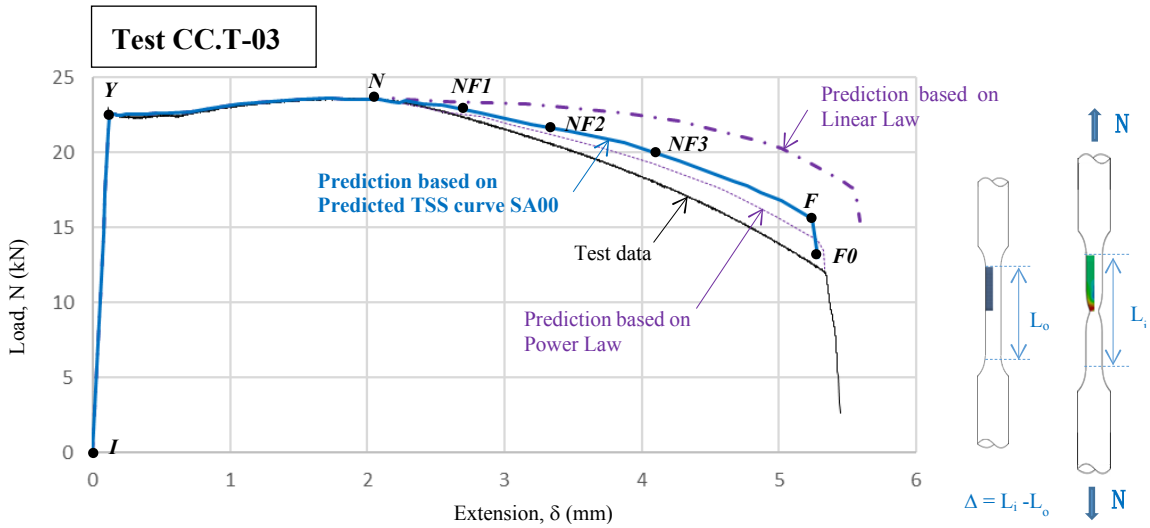

Figure 13: Load-extension curves of a S690 tensile test

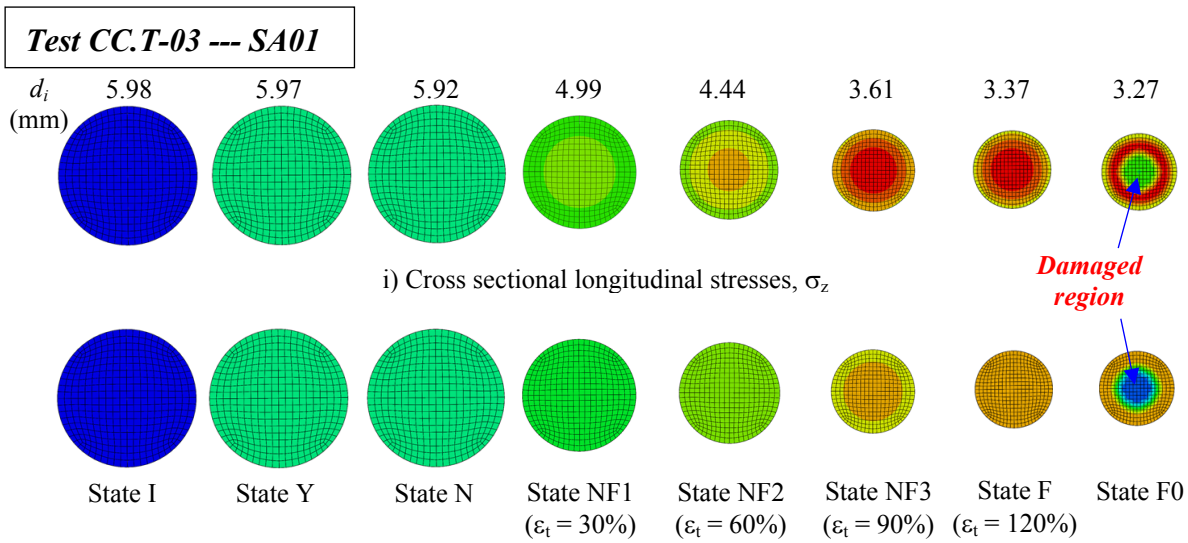

i) Cross sectional longitudinal stresses, σ_z

ii) Cross sectional von Mises stresses, σ_{vm}

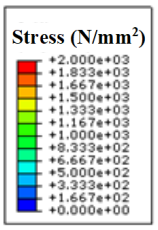

$$\eta_\sigma = \frac{\sigma_{vm,max}}{\sigma_{av}}$$

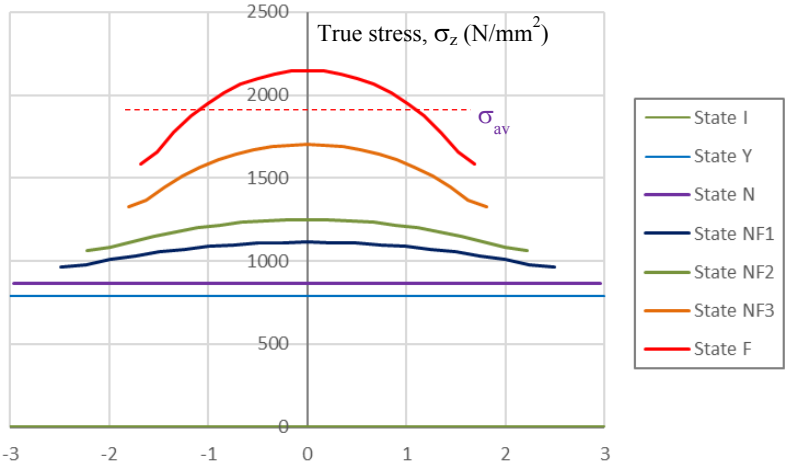

Transverse distance from the centre line of the minimum cross-section (mm)

iii) Variations of longitudinal stresses along the centre line

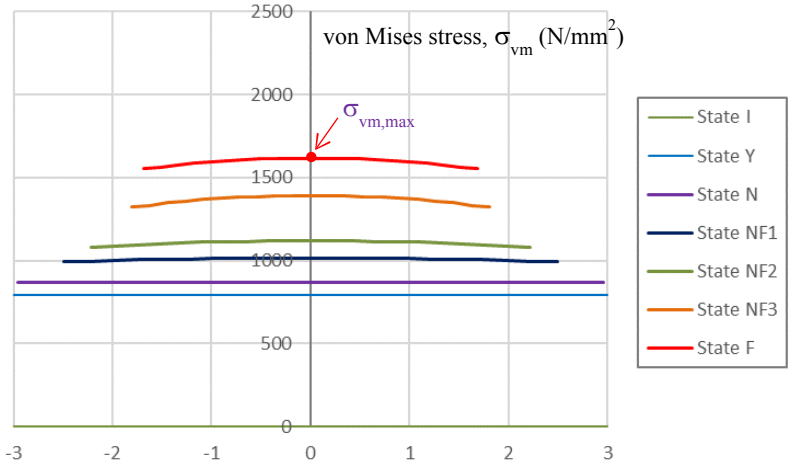

Transverse distance from the centre line of the minimum cross-section (mm)

iv) Variations of the von Mises stresses along the centre line

a) First approximation SA01

Figure 14: True stress distributions of the critical cross-section at various deformation states: Test CC.T-03

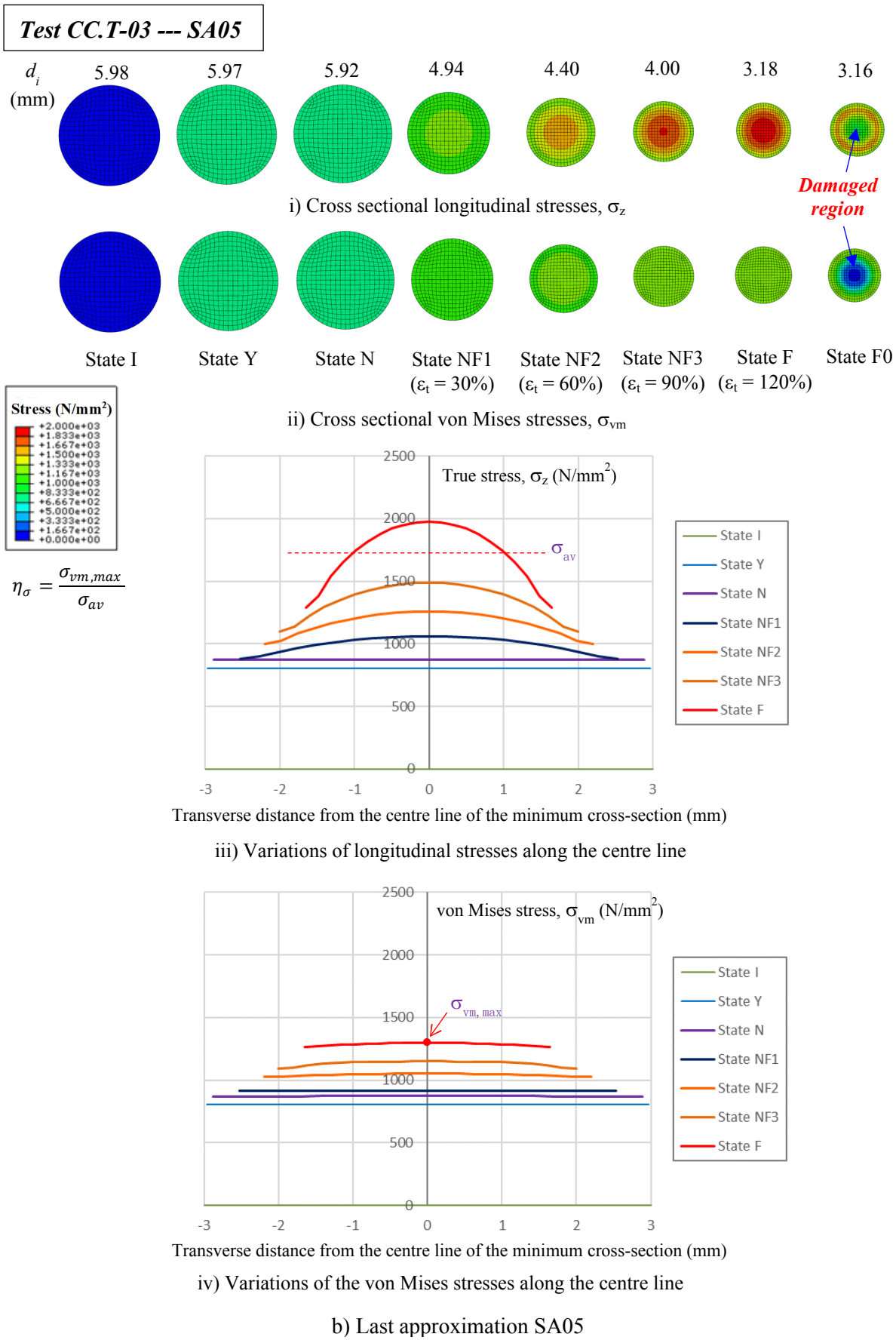

b) Last approximation SA05

Figure 14: True stress distributions of the critical cross-section at various deformation states: Test CC.T-03

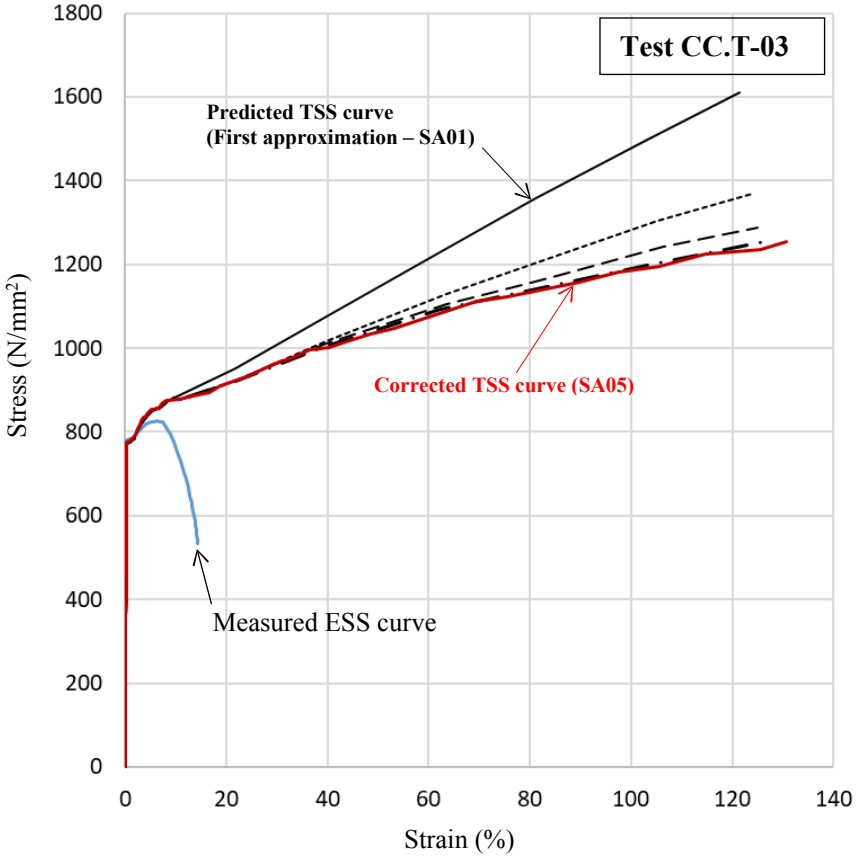

a) Predicted true stress-strain curves at various approximations

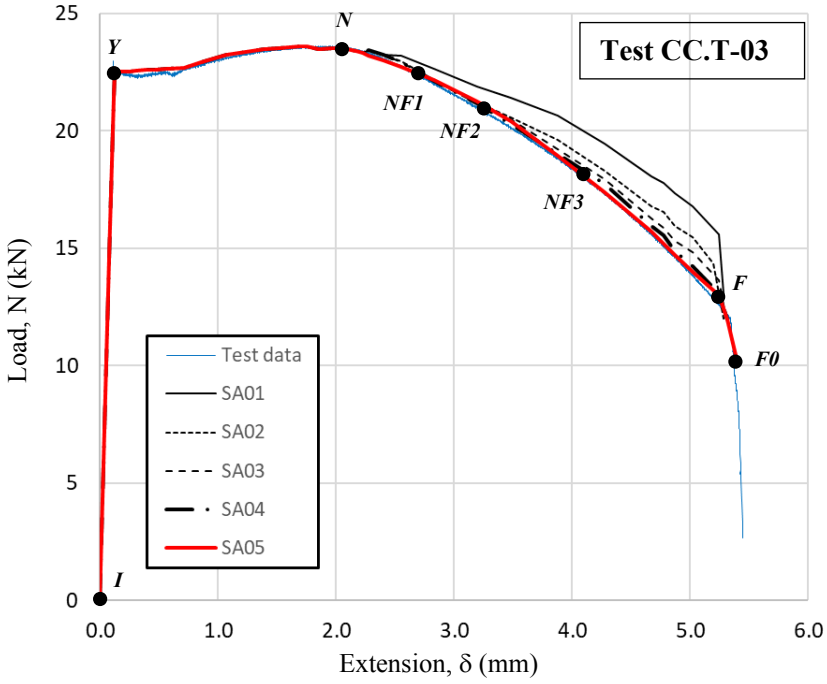

b) Predicted load extension curves at various approximations

Figure 15: Predicted load-extension curves through successive approximations

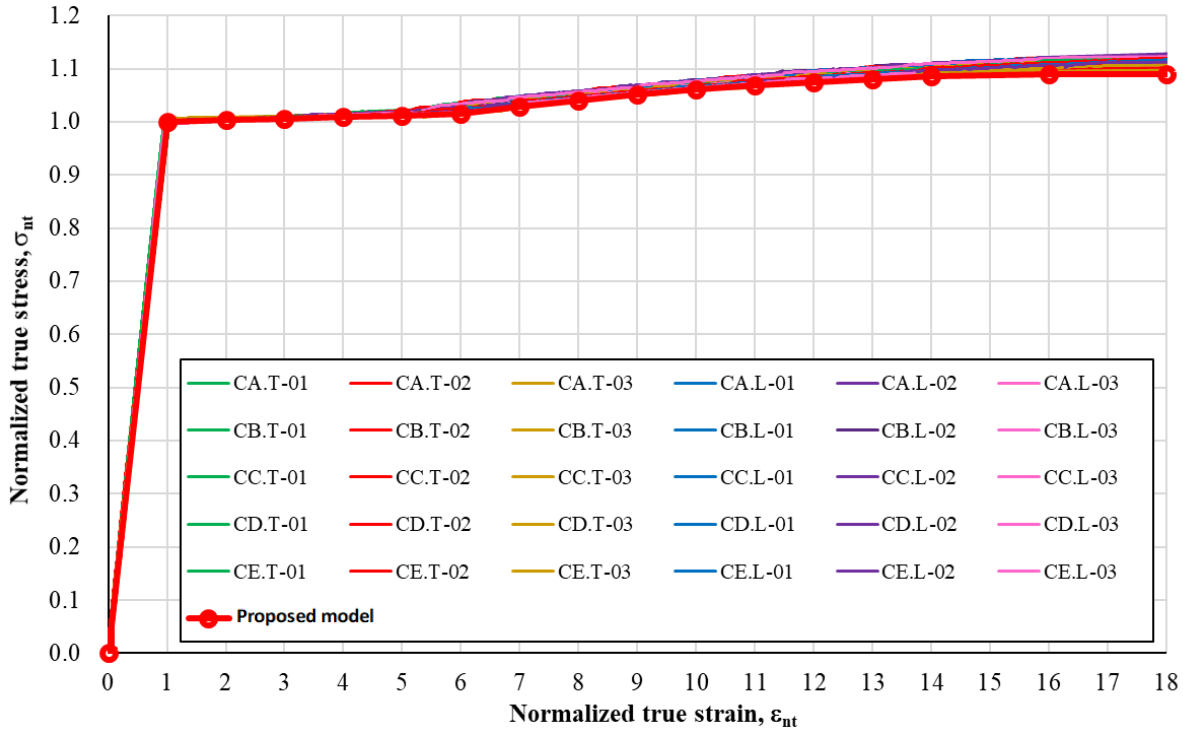

a) Normalized true stress-strain curves up to $\varepsilon_{nt} = 18$

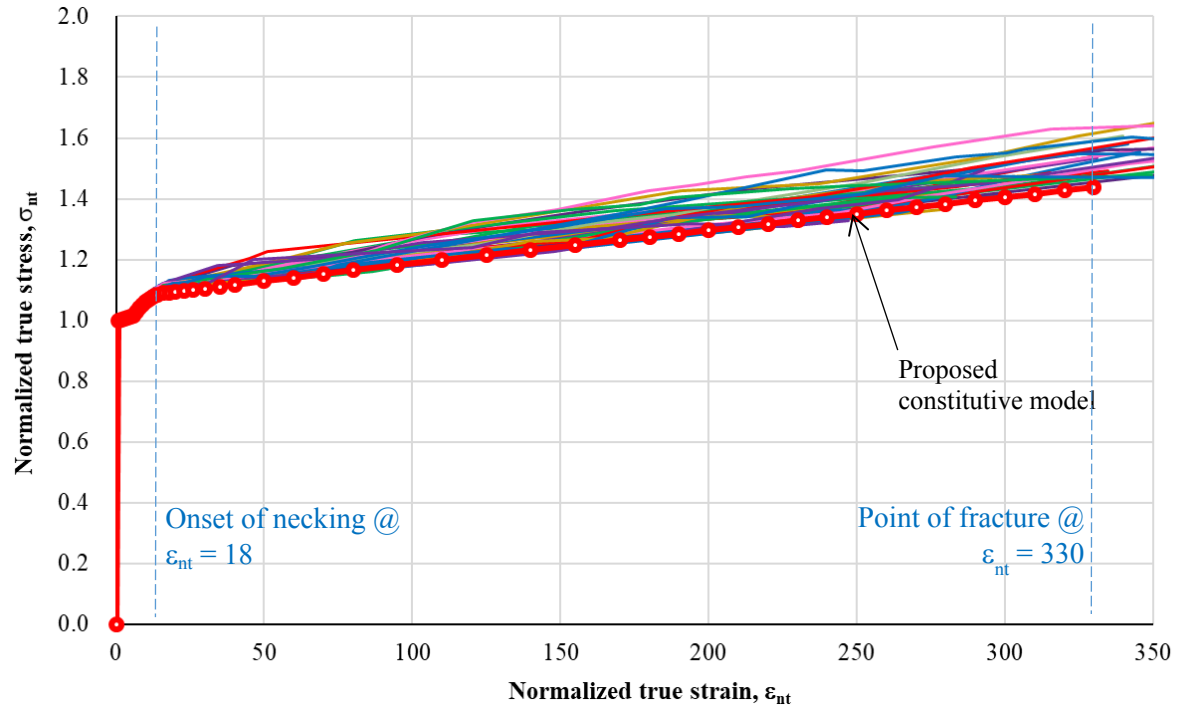

b) Full range normalized true stress-strain curves

Figure 16: Proposed normalized true stress-strain (σ_{nt} - ε_{nt}) curves

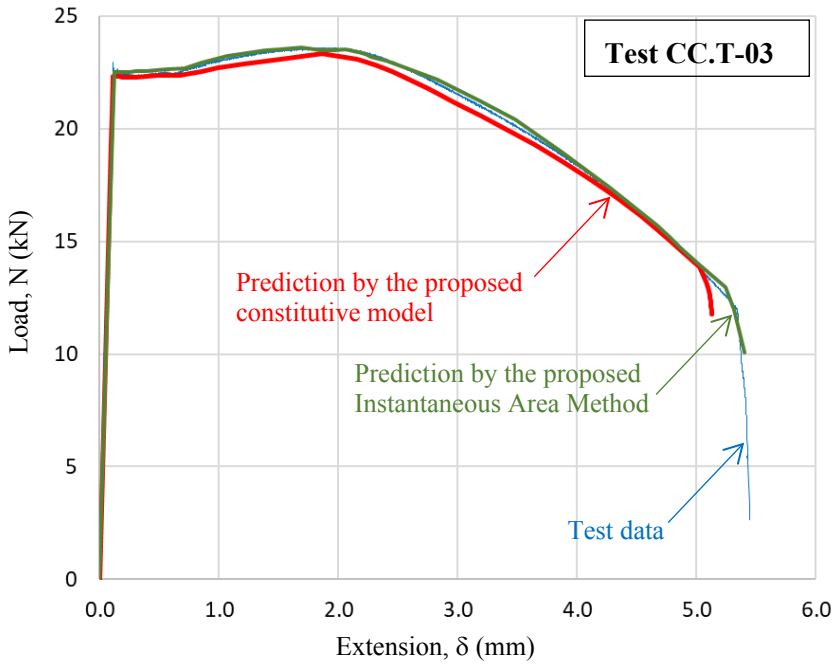

Figure 17: Predicted load extension curves using various constitutive models

Table 1 Chemical compositions of different S690 steel plates

	C (%)	Si (%)	Mn (%)	P (%)	S (%)	N (%)	B (%)	Cr (%)	Cu (%)	Mo (%)	Nb (%)	Ni (%)	Ti (%)	V (%)	Zr (%)
EN 10025-6	0.220	0.86	1.8	0.025	0.012	0.016	0.006	1.60	0.55	0.74	0.070	2.1	0.07	0.14	0.17
Plate A	0.137	0.22	1.38	0.010	0.001	0.004	0.00012	0.33	0.49	0.24	0.026	0.037	0.012	-	-
Plate B	0.130	0.25	1.40	0.015	0.001	0.001	0.00017	0.28	-	0.17	0.027	0.010	0.015	-	-
Plate C	0.130	0.26	1.39	0.011	0.001	0.002	0.00017	0.27	-	0.17	0.027	-	0.015	-	-
Plate D	0.080	0.26	1.61	0.012	0.001	-	0.00016	0.26	-	0.30	0.026	-	0.015	-	-
Plate E	0.090	0.26	1.61	0.013	0.001	-	0.00017	0.26	-	0.27	0.026	-	0.015	-	-

Table 2 Test programme of monotonic tensile tests

Test	Direction	Diameter (mm)	Cross-sectional area (mm^2)
CA.T-01	Transverse	6.00	28.27
CA.T-02	Transverse	6.00	28.27
CA.T-03	Transverse	6.00	28.27
CA.L-01	Longitudinal	6.02	28.46
CA.L-02	Longitudinal	6.00	28.46
CA.L-03	Longitudinal	5.98	28.09
CB.T-01	Transverse	5.97	28.01
CB.T-02	Transverse	5.96	27.85
CB.T-03	Transverse	5.96	28.11
CB.L-01	Longitudinal	5.98	28.11
CB.L-02	Longitudinal	5.93	27.66
CB.L-03	Longitudinal	5.99	28.14
CC.T-01	Transverse	5.98	28.09
CC.T-02	Transverse	5.98	28.09
CC.T-03	Transverse	5.98	28.09
CC.L-01	Longitudinal	5.98	28.09
CC.L-02	Longitudinal	5.98	28.09
CC.L-03	Longitudinal	5.98	28.09
CD.T-01	Transverse	6.00	28.27
CD.T-02	Transverse	6.00	28.27
CD.T-03	Transverse	5.98	28.09
CD.L-01	Longitudinal	5.96	27.90
CD.L-02	Longitudinal	5.96	27.90
CD.L-03	Longitudinal	5.98	28.09
CE.T-01	Transverse	6.00	28.27
CE.T-02	Transverse	6.00	28.27
CE.T-03	Transverse	6.00	28.27
CE.L-01	Longitudinal	5.96	27.90
CE.L-02	Longitudinal	5.98	28.09
CE.L-03	Longitudinal	5.96	27.90

Table 3. Loading rates for monotonic tensile tests

Stage	Purpose	Loading rates	
		BS EN ISO 6892-1 / *ASTM E8/E8M*	Test
1	Determination of E	360 ~ 3600 $N/mm^2/min$ *69 ~ 690 $N/mm^2/min$*	10 ~ 50 $N/mm^2/min$
2	Determination of f_y	0.015 ± 0.003 mm/mm/min *0.015 ± 0.006 mm/mm/min*	0.0002 ~ 0.0015 mm/mm/min
3	Determination of f_u	0.15 ± 0.03 mm/mm/min *0.05 ~ 0.5 mm/mm/min*	0.002 ~ 0.012 mm/mm/min
4	Determination of ε_L	0.15 ± 0.03 mm/mm/min *0.05 ~ 0.5 mm/mm/min*	0.002 ~ 0.012 mm/mm/min

Table 4. Deformations in a tensile coupon by digital photo analyses

Deformations	**Point I** Initial condition	**Point Y** Yield condition	**Point N** Necking condition	**Point F** Fracture condition
Digital Photos	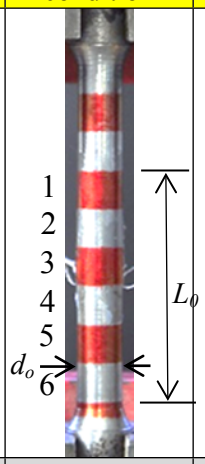	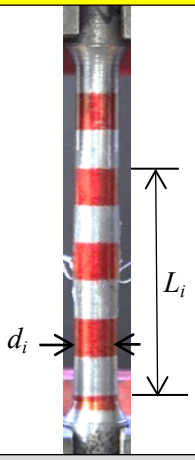	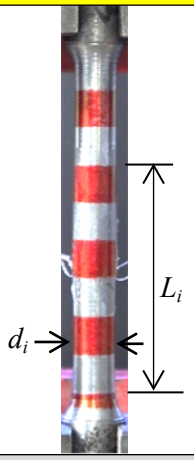	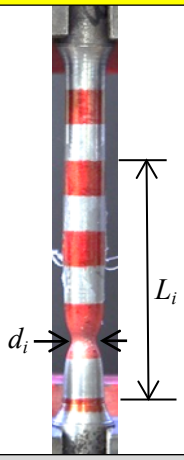
Overall gauge at 30.0 mm				
d_i (pixel)	410	409	398	209
d_i (mm)	6.00	5.99	5.82	3.06
L_i (pixel)	2160	2168	2300	2545
L_i (mm)	30.00	30.11	31.94	35.36
Strain (%)	0.00	0.37	6.49	17.87
Local gauge at 5.0 mm		Strain (%)	Strain (%)	Strain (%)
Segment No. 1	---	0.00	6.30	5.67
Segment No. 2	---	0.75	6.40	5.75
Segment No. 3	---	0.00	6.50	5.72
Segment No. 4	---	0.77	6.65	8.51
Segment No. 5	---	0.00	6.49	69.04
Segment No. 6	---	1.16	6.56	9.14
Strain measured by strain gauges		0.36	6.49	---

Table 5 Test results of monotonic tensile tests

Test	Yield strength f_y (N/mm^2)	Young's modulus E (kN/mm^2)	Tensile strength f_u (N/mm^2)	Strain at f_u ε_u (%)	f_u / f_y	15 ε_y (%)	Strain at fracture ε_L (%)
CA.T-01	711	209	753	5.5	1.06	5.1	18.1
CA.T-02	724	213	766	6.5	1.06	5.1	18.1
CA.T-03	733	229	768	6.4	1.05	4.8	17.2
CA.L-01	735	216	774	6.8	1.05	5.1	17.6
CA.L-02	735	218	773	6.3	1.05	5.1	17.9
CA.L-03	748	223	782	5.1	1.05	5.0	17.3
Average	***731***	***218***	***769***	***6.1***	***1.05***	***5.0***	***17.7***
St. Dev.	***12.5***	***7.1***	***9.6***	***0.7***	***0.0***	***0.1***	***0.4***
C.O.V.	***0.02***	***0.03***	***0.01***	***0.11***	***0.00***	***0.02***	***0.02***
CB.T-01	764	215	799	5.4	1.05	5.3	16.5
CB.T-02	761	221	796	6.0	1.05	5.2	15.9
CB.T-03	751	217	788	5.3	1.05	5.2	15.6
CB.L-01	757	217	791	5.2	1.05	5.2	17.8
CB.L-02	755	215	789	5.3	1.05	5.3	16.3
CB.L-03	763	215	799	5.4	1.05	5.4	17.1
Average	***758***	***217***	***793.4***	***5.4***	***1.05***	***5.27***	***16.52***
St. Dev.	***5.0***	***2.4***	***5.1***	***0.3***	***0.0***	***0.1***	***0.8***
C.O.V.	***0.01***	***0.01***	***0.01***	***0.05***	***0.00***	***0.02***	***0.05***
CC.T-01	756	213	796	7.4	1.05	5.3	18.2
CC.T-02	756	213	800	6.5	1.06	5.3	18.5
CC.T-03	759	212	799	6.5	1.05	5.4	15.6
CC.L-01	759	215	815	7.4	1.07	5.3	19.0
CC.L-02	759	217	800	8.1	1.05	5.3	17.7
CC.L-03	755	212	802	7.9	1.06	5.3	18.7
Average	***758***	***214***	***802***	***7.3***	***1.06***	***5.3***	***17.9***
St. Dev.	***1.6***	***1.7***	***6.6***	***0.7***	***0.0***	***0.0***	***1.2***
C.O.V.	***0.00***	***0.01***	***0.01***	***0.09***	***0.01***	***0.01***	***0.07***
CD.T-01	805	219	845	6.1	1.05	5.5	17.3
CD.T-02	806	208	857	6.8	1.06	5.8	16.9
CD.T-03	799	224	842	8.3	1.05	5.3	17.4
CD.L-01	798	217	833	6.5	1.05	5.5	17.9
CD.L-02	804	215	845	8.3	1.05	5.6	18.1
CD.L-03	797	212	846	6.7	1.06	5.6	19.6
Average	***801***	***216***	***845***	***7.1***	***1.05***	***5.6***	***17.9***
St. Dev.	***4.1***	***5.5***	***7.5***	***1.0***	***0.0***	***0.2***	***0.9***
C.O.V.	***0.01***	***0.03***	***0.01***	***0.13***	***0.00***	***0.03***	***0.05***
CF.T-01	801	210	845	8.0	1.05	5.7	17.3
CE.T-02	801	215	852	6.8	1.06	5.6	16.0
CE.T-03	801	215	852	6.8	1.06	5.6	16.0
CE.L-01	797	214	856	6.4	1.07	5.6	17.4
CE.L-02	801	215	855	7.5	1.07	5.6	17.8
CE.L-03	797	212	846	6.7	1.06	5.6	17.6
Average	***800***	***213***	***851***	***7.0***	***1.06***	***5.6***	***17.0***
St. Dev.	***2.1***	***1.9***	***4.6***	***0.6***	***0.0***	***0.1***	***0.8***
C.O.V.	***0.00***	***0.01***	***0.01***	***0.09***	***0.70***	***0.01***	***0.05***
Average	**770**	**215**	**812**	**6.6**	**1.06**	**5.4**	**17.4**
St. Dev.	*28.2*	*4.4*	*32.3*	*1.0*	*0.0*	*0.2*	*1.0*
C.O.V.	*0.04*	*0.02*	*0.04*	*0.15*	*0.01*	*0.04*	*0.06*

Table 6 Stress and strain correction factors of Coupon CC.T-03 at different deformation ranges

Successive approximation	Point N	Point NF1	Point NF2	Point NF3	Point F
	Stress correction factor, η_σ				
SA01	1.00	1.00	1.00	1.00	1.00
SA02	1.00	0.99	0.96	0.92	0.82
SA03	1.00	0.99	0.95	0.89	0.80
SA04	1.00	0.99	0.93	0.87	0.78
SA05	1.00	0.99	0.93	0.87	0.78
	Strain correction factor, η_ε				
SA01	1.00	1.00	1.00	1.00	1.00
SA02	1.00	1.00	1.01	1.02	1.05
SA03	1.00	1.01	1.01	1.03	1.10
SA04	1.00	1.01	1.03	1.08	1.18
SA05	1.00	1.01	1.03	1.08	1.18